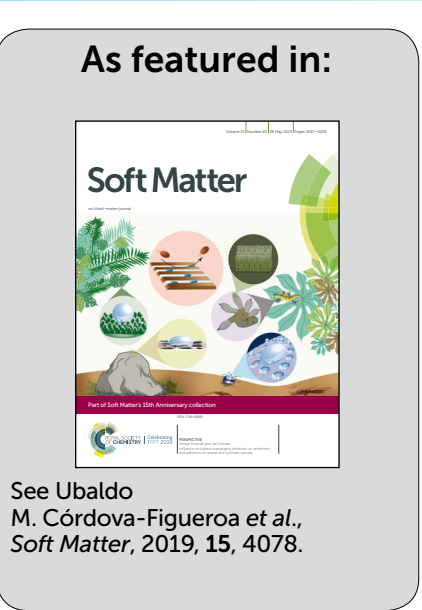


Highlighting research from the group of Prof. Ubaldo M. Córdova-Figueroa.

Self-assembly of magnetic colloids with shifted dipoles

Dilute suspensions of magnetic colloids with laterally shifted dipoles are studied using computer simulations. The rate of formation of clusters and their structures are quantified for several dipolar shifts from the particle center.





Soft Matter



View Article Online PAPER



Cite this: Soft Matter, 2019, **15**, 4078

Received 21st December 2018, Accepted 28th March 2019

DOI: 10.1039/c8sm02591f

rsc.li/soft-matter-journal

Self-assembly of magnetic colloids with shifted dipoles†

Gabriel I. Vega-Bellido, 📭 a Ronal A. DeLaCruz-Araujo, 📭 a Ilona Kretzschmar 📭 and Ubaldo M. Córdova-Figueroa (1) *a

The self-assembly of colloidal magnetic Janus particles with a laterally displaced (or shifted), permanent dipole in a quasi-two-dimensional system is studied using Brownian dynamics simulations. The rate of formation of clusters and their structures are quantified for several values of dipolar shift from the particle center, which is nondimensionalized using the particle's radius so that it takes values ranging from 0 to 1, and examined under different magnetic interaction strengths relative to Brownian motion. For dipolar shifts close to 0, chain-like structures are formed, which grow at long times following a power law, while particles of shift higher than 0.2 generally aggregate in ring-like clusters that experience limited growth. In the case of shifts between 0.4 and 0.5, the particles tend to aggregate in clusters of 3 to 6, while for all shifts higher than 0.6 clusters rarely contain more than 3 particles due to the antiparallel dipole orientations that are most stable at those shifts. The strength of the magnetic interactions hastens the rate at which clusters are formed; however, the effect it has on cluster size is lessened by increases in the shift of the dipoles. These results contribute to better understand the dynamics of magnetic Janus particles and can help the synthesis of functionalized materials for specific applications such as drug delivery.

1 Introduction

Magnetic colloids are of particular interest in the field of materials science due to the ease with which the structures formed can be controlled when their magnetic interactions are properly tuned. Nanoparticles of this nature have found myriad applications in progressive technologies such as photonics,¹ controlled motion,²⁻⁵ cancer treatment,⁶ and many others.⁷ To be able to design systems of magnetic colloids which can be easily controlled by exploiting their magnetic properties, we must first understand their aggregation dynamics based on the nature of the colloids.

The simplest model for the study of magnetic colloids is that of the dipolar hard sphere (DHS), a sphere of diameter d with a point dipole moment m located in the center, because of its isotropic shape and simple potential.8-11 The DHS model has been extensively studied, and its equilibrium properties are well understood. Variations on the DHS model can be introduced by adding shape or potential anisotropy. These variations produce differences in structure and macroscopic behavior, the study of which is the next step in understanding systems of magnetic colloidal particles. The subject of this study is one such variation on the DHS model, characterized by a lateral shifting of the dipole with respect to the particle center, commonly called the magnetic Janus particle. Similar systems of Janus particles are of great interest in the field of colloids due to their unique aggregation dynamics.12

Modern fabrication methods such as surface or bulk modification have been used to successfully produce magnetic Janus particles. 13,14 One version of this method consists of using vapor deposition to coat patches of the particle with a metal such as iron oxide, thereby inducing a magnetic dipole on the particle. Studies have shown that varying the deposition rate causes the particles to exhibit distinct assembly behaviors in a way analogous to the shifting of a dipole. 15,16 This proves that there are ways to tune the dipole of a magnetic colloidal particle, and as such it is important to understand the structures which pertain to each dipolar shift and magnetic potential, so as to predict these structures in a real-world environment.

Previous research on these particles has mostly focused on the effects that polydispersity, shape anisotropy, and dipole placement have on the equilibrium behavior of the system. 17-21 Studies of large systems of Janus particles through the use of molecular dynamics simulations have been conducted,22 but these also focused on equilibrium behavior. Only recently have studies begun to delve into the dynamic aspects of these

^a Department of Chemical Engineering, University of Puerto Rico - Mayagüez, Mayagüez, PR 00681, USA. E-mail: ubaldom.cordova@upr.edu

^b Department of Chemical Engineering, City College of New York, City University of New York, NY 10031, USA

[†] Electronic supplementary information (ESI) available: Videos of the systems presented in Fig. 3, population distributions for higher concentrations, orientation distributions for systems of low shift as a function of λ , and radius of gyration as a function of cluster size. See DOI: 10.1039/c8sm02591f

Paper Soft Matter

systems, such as the relaxation dynamics of systems driven by time-dependent magnetic or electric fields and the control of self-propelled systems.^{23–25} Previous work has shown that an increasing dipolar shift causes the ground state structures of the system to transition from chain-like to ring-like aggregates, ²⁶ with increasing dipoles leading to more compact structures, but the dynamic growth and distribution of the structures in these systems has not been reported on.

The purpose of this work is to explore the effect a Janus nature has on the dynamics of quasi-two-dimensional magnetic particle self-assembly. The growth of these systems was quantified by studying the average cluster size and system nucleation over time, with systems being categorized based on when they reach equilibrium. Characteristic structures of the system at equilibrium were also studied by way of inter-dipolar angles and population distributions. Circularity of clusters was also determined by measuring effective radius as a function of cluster size and comparing values to the effective radius of an ideal chain or circle. This article is organized as follows: in the Problem formulation section the model is introduced, along with the governing equations for the system and the parameters studied. In the Results section we present the simulation results, including graphs for dynamic cluster growth and equilibrium system structures. In the Conclusions section we draw conclusions and discuss plans for future work.

2 Problem formulation

2.1 Model

The model consists of identical colloidal particles with a permanent laterally shifted dipole modeled as hard spheres submerged in a quasi-two-dimensional Newtonian fluid at constant temperature. Fig. 1 shows the model system where \mathbf{m}_i and \mathbf{m}_i are the dipolar moments, S is the distance of the dipoles from the particle center, and a is the particle radius. This figure also showcases the primed reference system (x', y', z') individual to each particle and the laboratory reference system universal to the simulation. Particles are initialized with random positions and orientations in a periodic box with a surface fraction ϕ_s = 0.01. Because of their associated computational cost, and since they have been shown to strictly slow down kinetics in the nucleation process and speed it up in the growth process for a dilute system, 27,28 hydrodynamic interactions are not accounted for in this model. The dipolar shift is found dividing the absolute shift S by the particle radius a, i.e., s = S/a. This model is representative of Janus particles with a ferromagnetic cap moving between two glass slides, a common way to study such particles experimentally.

2.2 Governing equations

Considering the particles are subjected solely to Brownian motion, interparticle forces, and hydrodynamic drag, the following overdamped Langevin equations for the forces and torques arise:

$$\mathbf{F}^{\mathbf{D}} + \mathbf{F}^{\mathbf{P}} + \mathbf{F}^{\mathbf{B}} = 0, \tag{1}$$

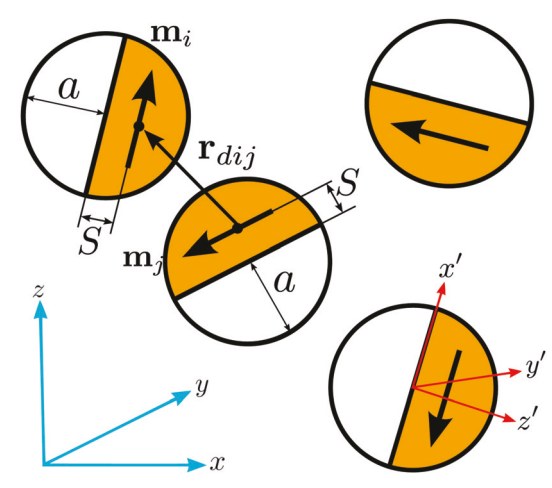


Fig. 1 Model system. The magnetic region of the spherical colloids is represented in orange given a magnetic dipole moment (m; or m;) laterally displaced a distance S from the particle center. The body fixed (x', y', z')and the laboratory reference (x, y, z) frames, and additional interparticle interaction parameters are also shown.

$$\mathbf{T}^{\mathbf{D}} + \mathbf{T}^{\mathbf{M}} + \mathbf{T}^{\mathbf{B}} = 0, \tag{2}$$

where FD and TD are the drag force and torque, FD is the summation of forces due to magnetic and repulsive interactions between particles, T^M is the torque due to magnetic interactions, and FB and TB are the Brownian force and torque. The magnetic interaction force is modeled by the dipole-dipole interaction potential:

$$\Phi_{\mathrm{dd}}(\mathbf{r}_{\mathrm{d}ij}) = -\frac{\mu_0}{4\pi} \left[3 \frac{\left(\mathbf{m}_i \cdot \mathbf{r}_{\mathrm{d}ij} \right) \left(\mathbf{m}_j \cdot \mathbf{r}_{\mathrm{d}ij} \right)}{r_{\mathrm{d}ij}^5} - \frac{\left(\mathbf{m}_i \cdot \mathbf{m}_j \right)}{r_{\mathrm{d}ij}^3} \right], \tag{3}$$

$$\mathbf{r}_{\mathrm{d}ij} = \mathbf{r}_{\mathrm{d}i} - \mathbf{r}_{\mathrm{d}j}, \quad r_{\mathrm{d}ij} = |\mathbf{r}_{\mathrm{d}ij}|,$$
 (4)

where μ_0 is the vacuum permeability $(4\pi \times 10^{-7} \text{ H m}^{-1})$, and r_{dii} is the dipole-dipole distance. The repulsive Weeks-Chandler-Andersen (WCA)²⁹ potential used to model steric repulsion between particles is given by:

$$\Phi_{\text{WCA}}(r_{ij}) = \begin{cases} 4\varepsilon \left[\left(\frac{2a}{r_{ij}} \right)^{12} - \left(\frac{2a}{r_{ij}} \right)^{6} \right], & \text{if } r_{ij} \le 2^{1/6} 2a, \\ 0, & \text{if } r_{ij} > 2^{1/6} 2a \end{cases}$$

where ε is the potential strength, a is the particle's radius, and r_{ij} is the distance between particle centers of mass.

Upon integration over finite differences of eqn (1) and (2), the resulting nondimensionalized equations of motion for particle position and orientation arise:

$$\tilde{\mathbf{r}}(\tilde{t} + \Delta \tilde{t}) = \tilde{\mathbf{r}}(\tilde{t}) + \tilde{\mathbf{F}}^{P}(\tilde{t})\Delta \tilde{t} + \Delta \tilde{\mathbf{r}}^{B}, \tag{5}$$

$$\mathbf{\Omega}(\tilde{t} + \Delta \tilde{t}) = \mathbf{\Omega}(\tilde{t}) + \tilde{\mathbf{T}}^{\mathrm{M}}(\tilde{t})\Delta \tilde{t} + \Delta \mathbf{\Omega}^{\mathrm{B}}, \tag{6}$$

where $\Delta \tilde{\mathbf{r}}^{\mathrm{B}}$ and $\Delta \mathbf{\Omega}^{\mathrm{B}}$ are the random displacements inducing the translational and rotational Brownian motion, respectively. In these equations, the lengths were scaled with the particle radius $(r \sim a)$, the time was scaled with the characteristic diffusion time ($t \sim \tau_{\rm D}$), the forces were scaled using the Brownian force ($F \sim k_{\rm B}T/a$), and the torques with the Brownian torque ($T \sim k_{\rm B}T$).

The Brownian displacement and rotation contributions in eqn (5) and (6) can be characterized by the following statistical properties:

$$\langle \Delta \tilde{\mathbf{r}}^{\mathrm{B}} \rangle = 0, \quad \langle \Delta \tilde{\mathbf{r}}^{\mathrm{B}} \Delta \tilde{\mathbf{r}}^{\mathrm{B}} \rangle = 2\mathbf{I}\Delta \tilde{t},$$
 (7)

$$\langle \Delta \mathbf{\Omega}^{\mathrm{B}} \rangle = 0, \quad \langle \Delta \mathbf{\Omega}^{\mathrm{B}} \Delta \mathbf{\Omega}^{\mathrm{B}} \rangle = 3/2 \mathbf{I} \Delta \tilde{t}.$$
 (8)

In order to properly track the rotation of the particle dipoles in three dimensional space, the quaternion parameters χ , η , ξ , and ζ are used to define their orientation. Using these quaternions we define the transformation matrix **A** as in:^{30,31}

$$\mathbf{A} = \begin{pmatrix} -\xi^2 + \eta^2 - \zeta^2 + \chi^2 & 2(\zeta\chi - \xi\eta) & 2(\eta\zeta + \xi\chi) \\ -2(\xi\eta + \zeta\chi) & \xi^2 - \eta^2 - \zeta^2 + \chi^2 & 2(\eta\chi - \xi\zeta) \\ 2(\eta\zeta - \xi\chi) & -2(\xi\zeta + \eta\chi) & -\xi^2 - \eta^2 + \zeta^2 + \chi^2 \end{pmatrix}.$$

The magnetic torque on the particles primed reference system is obtained with $\mathbf{T}^{\mathbf{M}\prime} = \mathbf{A}\cdot\mathbf{T}^{\mathbf{M}}$. This magnetic torque is used to find the principle axis angular velocity by dividing the changing orientation portion of eqn (6) by the time step, $\Delta \mathbf{t}$. The time evolution of the quaternions is related to the principle axis angular velocity, ω' , via the following matrix:^{30,31}

$$\begin{pmatrix} \dot{\xi} \\ \dot{\eta} \\ \dot{\zeta} \\ \dot{\chi} \end{pmatrix} = \frac{1}{2} \begin{pmatrix} -\zeta & \chi & \xi & \eta \\ -\chi & -\zeta & \eta & \xi \\ \eta & -\xi & \chi & -\zeta \\ \xi & \eta & \zeta & \chi \end{pmatrix} \begin{pmatrix} \omega_x' \\ \omega_y' \\ \omega_z' \\ 0 \end{pmatrix}.$$

2.3 Parameters used

The strength of the magnetic interaction potential between particles is dictated by the dipolar coupling constant λ , a dimensionless parameter, which represents the ratio of magnetic to Brownian forces and is defined as:

$$\lambda = \frac{\mu_0 m^2}{4\pi a^3 k T}. (9)$$

For the repulsive WCA potential, we varied the energy parameter ε depending on the strength of the magnetic interactions.

The values studied for shift range from 0.0–0.6 as it has been shown by Yener and Klapp²² that higher values yield few new insights and are not experimentally relevant. An emphasis is given to small shifts due to the substantial change in cluster properties for shifts smaller than 0.2. The results shown are for λ = 15–45, values lower than this were shown to not produce any aggregation, while values higher than 75 caused all systems to exhibit system size dependence through cluster agglomeration. In order to resolve the fastest time scale in the system, which is the characteristic diffusion time of the particles $\tau_{\rm D}$, the time step is nondimensionalized using it, *i.e.*, $\Delta \tilde{t} = \Delta t/\tau_{\rm D}$. For low and medium shift cases the time step is kept at 10⁻⁴, but it is increased for simulations in which the shift is higher than 0.5 due to the strength of the magnetic potential rising sharply when the distance between dipoles is smaller than 1. The WCA

potential energy parameter ε is also only increased when the shift is higher than 0.5 in order to balance the sharply increasing magnetic potential. System size effects were studied in cases of small-shift by varying the amount of particles from 250–750, while systems of medium and high shift were kept at 500 particles since system-size effects are negligible for those cases.

2.4 Cluster properties

Two particles are considered to be in a cluster if the distance between their centers is below the interaction range, *i.e.*, $r_{ij}/2a < \alpha$. The value of the interaction range used in this work, to avoid misquantification of clusters (as linear or ring structures), is $\alpha = 1.2$. The unfolding method is used to account for the periodic boundary conditions. ^{32,33} Using the number of clusters $N_{\rm c}$ and the amount of particles in each cluster $N_{\rm c,p}$, the weight averaged mean cluster size can be calculated using the formula:

$$\langle N_{\rm c} \rangle = \left\langle \frac{\sum\limits_{p=1}^{N_{\rm c}} (N_{\rm c,p})^2}{\sum\limits_{p=1}^{N_{\rm c}} N_{\rm c,p}} \right\rangle. \tag{10}$$

In order to quantify the nucleation and growth phases, the nucleation factor is calculated for each system using the formula:

$$n_{\rm c} = \frac{N_{\rm c} - N_{\rm S}}{N_{\rm p}},\tag{11}$$

where $N_{\rm S}$ is the number of singlets in the simulation and $N_{\rm p}$ is the number of particles. It is important to note that for the purposes of this formula, singlets also count as clusters. The cluster size distribution $P(N_{\rm c})$ is also calculated.

2.5 Structure properties

In order to quantify the orientational ordering of the particles, the bonded particle orientation distribution function $P(\mathbf{m}_i \cdot \mathbf{m}_j)$ is calculated, considering that two particles are bonded as long as they satisfy the distance criterion described above. The effective radius of clusters as a function of cluster size is also studied as a means to gage the "circularity" of clusters.

3 Results

3.1 Dynamic cluster growth

We begin our discussion by showing some of the structures formed for various combinations of dipolar shift, a magnetic interaction potential strength of 45, and a surface fraction of 0.01 over the course of the simulation in Fig. 2. Qualitatively, three main cluster types can be observed for low (s = 0.0.1), medium (s = 0.2-0.5), and high dipolar shifts (s = 0.6-1). For low shifts, as shown in Fig. 2a–f, clusters tend to be in the form of long chains or large loops that continuously grow in size as the simulation progresses. It is expected that at very long times all particles would form part of a single cluster in these systems, hence the size of these clusters depends on the amount of particles simulated and the length of the simulation. At medium shifts, as shown in Fig. 2g–i, particles aggregate in compact

Paper Soft Matter

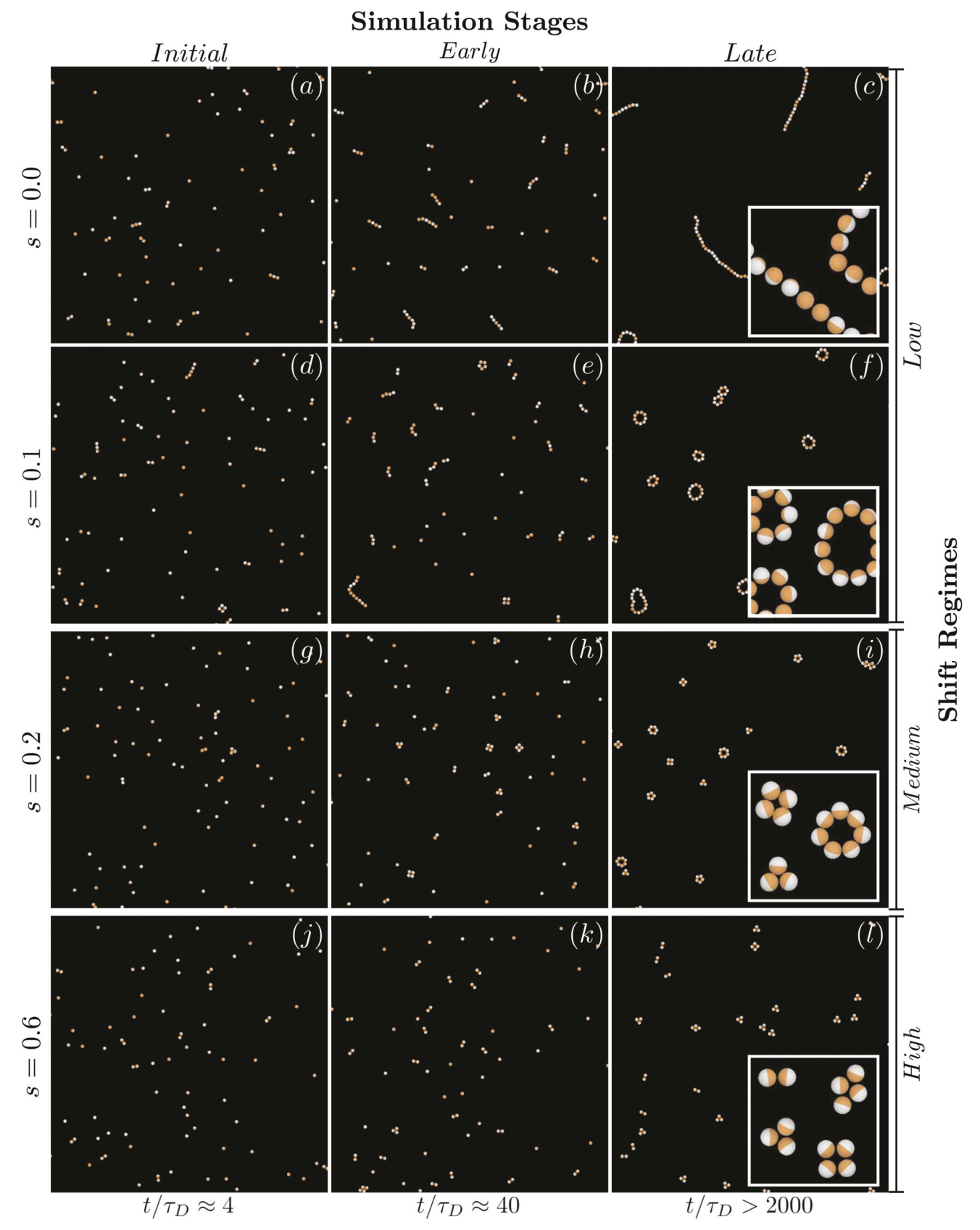


Fig. 2 Simulation renderings of systems of s = 0.0, 0.1, 0.2, and 0.6 over time. Panels (a), (d), (g), and (j) show overviews of the initial clusters formed. Panels (b), (e), (h), and (k) show the first signs of the clusters that characterize each system forming. Panels (c), (f), (i), and (l) contain overviews of the simulation at long times and closeups of each system's characteristic clusters. Magnetic dipoles are shifted into orange regions.

ringlike structures, which experience some growth throughout the simulation. At high shifts, as shown in Fig. 2j-l, mostly antiparallel doublets and triplets are present, as new particles rarely aggregate with existing triplet clusters. For all the renderings presented in Fig. 2: repulsive surfaces are shown in white, and magnetic surfaces are shown in orange; from left to right Fig. 2 follows a pattern of initial simulation snapshot $(t/\tau_D = 0)$, early simulation clusters snapshot ($t/\tau_D = 40$), and late simulation closeup ($t/\tau_{\rm D} > 2000$) of characteristic clusters. Videos of these systems can be found in the ESI.†

The ground state structures found by previous studies²⁶ match those seen for systems of medium and high shift.

In order to quantify the dynamic growth of the system, we graph the average cluster size and the nucleation factor over time, as seen in Fig. 3a and b. A distinction is made for systems of low shift by graphing them using open symbols due to their time-dependent nature. This nature is demonstrated by the fact that the system does not reach an equilibrium of average cluster sizes as the simulation progresses, but rather continues to increase following a power law behavior as clusters continue to acquire more particles. The continued growth of these systems is due to the chainlike configuration in which the particles bond that allows for easier bonding of particles as soon as they find themselves in the range of another particle's magnetic interaction potential. This continued growth is a characteristic of Diffusion Limited Aggregation (DLA), as particles bond irreversibly and the process is limited only by their mutual diffusion. Unlike DLA processes with isotropic potentials, clusters in Janus particle systems such as this one are not ramified, but rather consist of loose single chains of particles.

As the mean cluster size graph shows in Fig. 3a, the trend observed is that the average cluster size decreases as the shift

parameter increases, with the largest average cluster size of around 20 being reached by the lowest shift system of 0.0, and the smallest long time average cluster size of 3 pertaining to systems with a shift of 0.6. The trend of decreasing cluster size is caused by how the shift parameter affects the way particles bond. As the shift parameter increases, clusters begin to contract and the dipoles move towards the center of the cluster, making it difficult for new particles to enter clusters as the attractive forces between particles inside the cluster and those outside decrease greatly with increasing distance. The distance eventually causes attractive forces to be insufficient to overcome the potential barrier induced by the repulsive forces between particles. Because of this, systems of medium and high shift reach an equilibrium phase where the average cluster size ceases to increase. The equilibrium size is determined by a balance between aggregation due to magnetic attraction and dis-aggregation due to Brownian motion. This behavior is indicative of Reaction Limited Aggregation (RLA),34 and is the crucial distinction between high and the low-shift systems. For cases of $\lambda > 75$ cluster sizes continue to grow past the point where equilibrium is found in other systems, because the magnetic attraction becomes strong enough to overcome inter-particle repulsion regardless of particle orientation.

The nucleation graph in Fig. 3b shows the nucleation and growth phases for each system. The initial slope demonstrates particle-particle aggregation, the nucleation phase, where singlets begin to aggregate into clusters. Stable clusters in our systems aggregate irreversibly, and as such there will be almost no singlet particles at long times, when this point is reached it signals that the nucleation phase has ended. Past that, the particles experience cluster-cluster aggregation, the growth phase, where all particles form part of some cluster and clusters

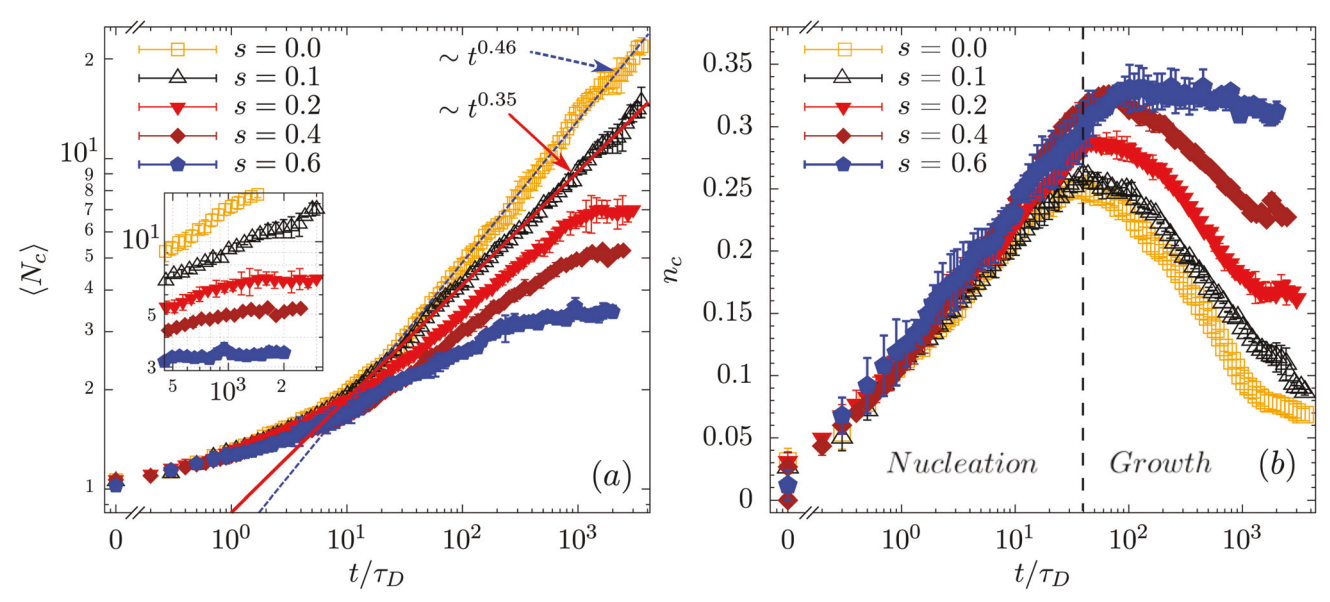


Fig. 3 Time effect on the aggregation behavior of a dilute system of magnetic Janus particles at $\lambda = 45$. Panel (a) shows weight averaged mean cluster size, $\langle N_c \rangle$, as a function of time for various s. Additionally, the continuous lines represent the power law aggregation behavior at long time. Panel (b) shows the nucleation and growth process for the same dipolar shifts, s, as presented in panel (a). In both panels filled symbols correspond to cases where we observe systems with time-independency, while open symbols correspond to systems that are time-dependent. This style is adhered to for all following graphs.

begin to aggregate with one another. For low shift systems, the growth phase will theoretically continue until all particles are part of one cluster, but the dilute nature of the simulation slows down the process such that it becomes too computationally taxing to achieve. Systems with medium shifts experience slower and limited growth due to their RLA nature, and eventually reach an equilibrium similar to the mean cluster size graph. For high shifts the basic doublet and triplet clusters do not experience much growth and as such the system quickly reaches equilibrium once nucleation ceases.

3.2 Population distribution

Paper

Fig. 4 contains the population distribution of clusters, which is used to study in detail the differences in aggregation behavior caused by the dipolar shift. The total time simulated is $\approx 3000\tau_D$ (see Fig. 3a) and the data in Fig. 4 represents the average of the last 20% of the simulations. Low shifts are graphed using open symbols in order to indicate their time-dependent nature, though it is clear that these systems create the largest clusters by a significant margin. It is clear that at longer times the population distributions would show the peaks just shifted to the right. For medium shifts, clusters can reach sizes of up to 12 for a shift of 0.2, but they generally consist of 3-8 particle clusters. For high shifts, cluster size varies very little, only from 2 to 4 particles, with a majority of clusters consisting of 2 or 3 particles. Increasing λ causes larger clusters to form, but the effect is most prominent for systems of low shift while being negligible for systems of high shift. These results coincide with the findings regarding the orientations of particles found in Fig. 5. The negligible amount of singlets for all cases also confirms that stable clusters in all systems studied aggregate irreversibly. In order to tune these distributions for systems that reach equilibrium, the surface fraction can be increased, leading to more clusters in the 4-8 particle region; but increasing the surface fraction also leads to increased cluster-cluster aggregation. Population distributions showing these behaviors can be found in the ESI† (Fig. S1).

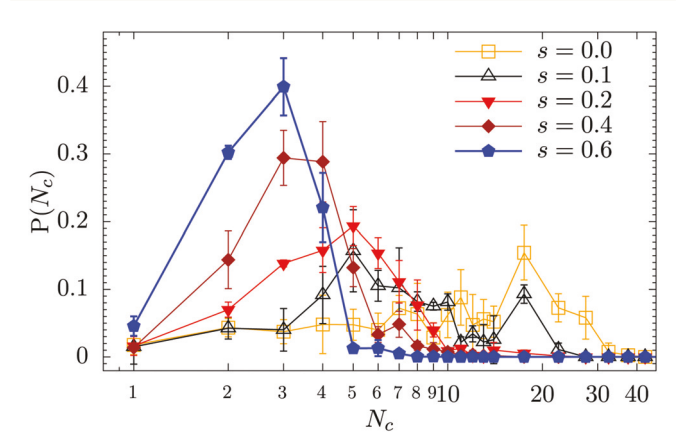


Fig. 4 Effect of shift on cluster size distributions, $P(N_c)$, for the same systems studied in Fig. 3. Filled symbols correspond to cases where the mean cluster size is time-independent, while open symbols correspond to cases where we observe time-dependency

3.3 Structural properties

Fig. 5 displays the distribution of dipole orientations for particles that share a cluster and the accompanying characteristic clusters for each system. Similar to Fig. 4, the data in Fig. 5 represents the average of the last 20% of the simulations. Systems with shifts of zero have a large peak at 1, indicating an angle of 0°. This angle corresponds to the chain configuration, which is the most stable state for bonded particles with a centered dipole. For systems with shift equal to 0.1 the distribution begins to slant towards values between 0.5 and 1, corresponding to angles between 45° and 0°, indicating that the clusters are beginning to contract and form amorphous, ring-like structures.

For shifts of 0.2, a spread of peaks are found between 0 and 1, indicating angles between 90° and 0°. These angles correspond to rings of 4 or more particles. The most common values for a shift of 0.4 are 0 and -0.5, corresponding to angles of 90° and 120° , indicating clusters of 4 and 3 particles, respectively. A 90° angle indicates a head-to-side orientation, meaning the particles dipoles arrange in a square formation. A 120° angle indicates that the particle dipoles arrange themselves in an equilateral triangle formation. For a shift of 0.6, there are very clear peaks at -0.5 and -1, indicating clusters of 3 and 2 particles respectively. Doublets and triplets are the most common structure for shifts higher than 0.6, with doublets becoming more probable as the shift approaches 1. For dipolar shifts in the range $0 \le s \le 0.5$, the WCA potential strength, ε , is kept at 100. This causes noticeable interpaticle separation at s = 0 (see Fig. 5b), which is reduced as s increases (see Fig. 5b, d, f and h). This is because as s increases the magnetic force increases (due to the magnetic dipoles being closer to each other), consequently, the equilibrium distance of the total interaction potential decreases. At s > 0.5, the magnetic force overcomes the WCA potential force for $\varepsilon = 100$, causing overlapping between particles. To avoid overlapping, ε was significantly increased (ε = 1000), leading to the increased distance between particles noticeable at s = 0.6 (see Fig. 5j), similar to that observed at s = 0.

This clearly shows the effect the dipolar shift has on the favored structures for each system, causing them to go from long chains, to ringlike structures, to triplets and doublets. Increasing λ did not have an effect on the orientation distribution of systems with $s \ge 0.1$, but for very low shift systems (s = 0.0 and 0.05) it led to a significantly higher portion of particles forming a straight chain, effectively increasing the rigidity of those clusters. A figure detailing these results can be found in the ESI† (Fig. S2).

Fig. 6 represents the effective radius of clusters as a function of cluster size throughout the aggregation process. The behavior of effective radius for straight chains ($R_{\text{eff,chains}}$) and ideally circular rings ($R_{\rm eff,rings}$), nondimensionalized with the particle radius a, is plotted using the following equations:

$$R_{\text{eff,chains}} = N_{\text{c}},$$
 (12)

$$R_{\rm eff,rings} = 1 + \frac{1}{\sin(\pi/N_{\rm c})}.$$
 (13)

Systems of 0.0 shift tend strongly towards chain-like behavior, and they exhibit large standard deviations in effective radius when clusters contain 15 or more particles due to the Soft Matter Paper

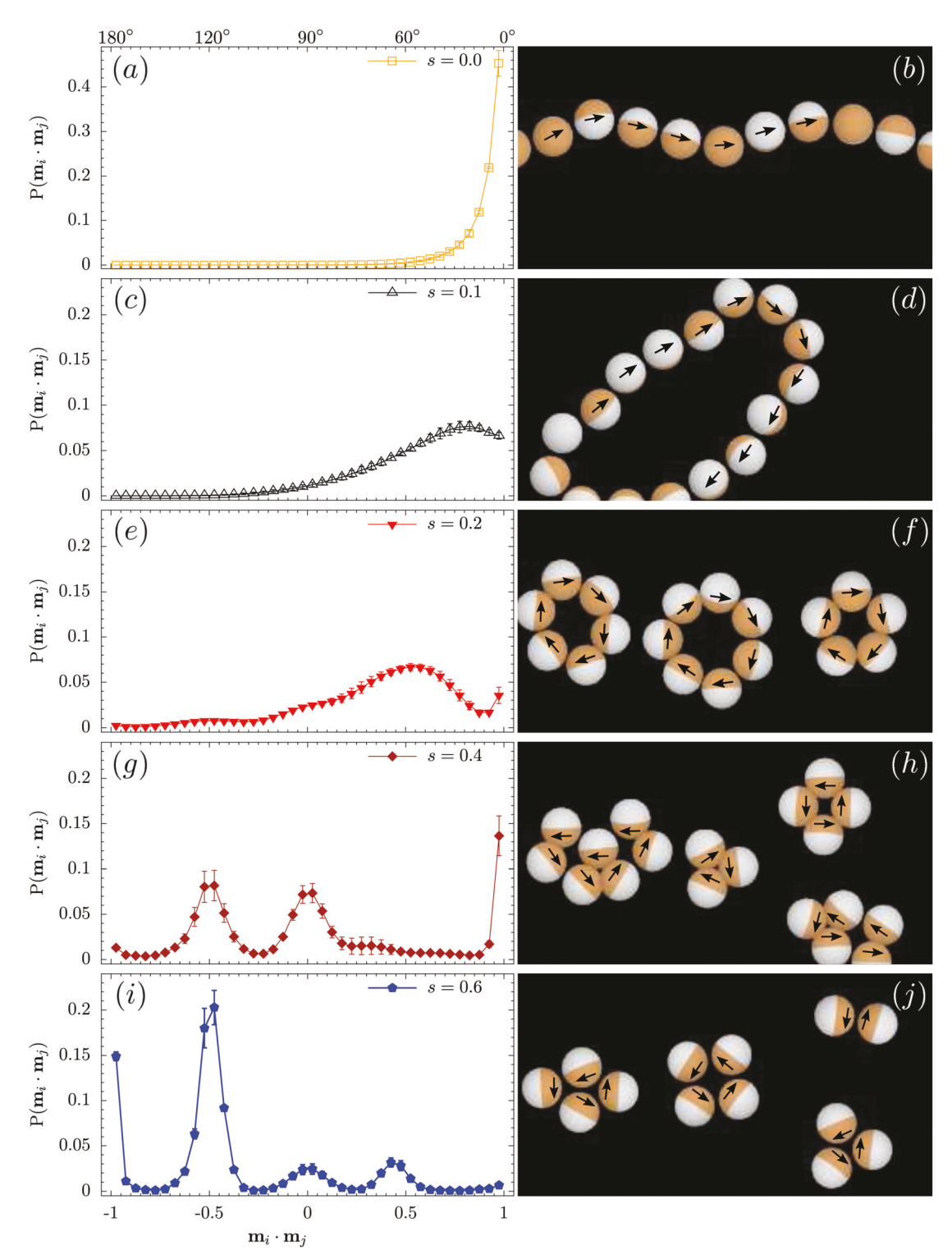


Fig. 5 Effect of shift on orientational distribution function. Panels (a), (c), (e), (g), and (i) demonstrate the bonded particle orientation distribution functions for the same five systems studied in Fig. 3. Panels (b), (d), (f), (h), and (j) contain the characteristic clusters for each of the systems.

Brownian forces randomly bending the chains, which is consistent with what is observed in the literature.²² For 0.05 shift the behavior is similar, up until around 15 particles, where effective radius decreases as clusters start transitioning into amorphous rings due to the dipole shift curving the clusters in a particular direction. At 0.1 shift, the transition from chains into rings occurs around a cluster size of 6 particles, and leads to more compact clusters than lower shift systems. Systems of shifts 0.2, 0.4, and 0.6 exhibit very similar behavior, forming compact clusters that hardly deviate from ideally circular

Paper Soft Matter

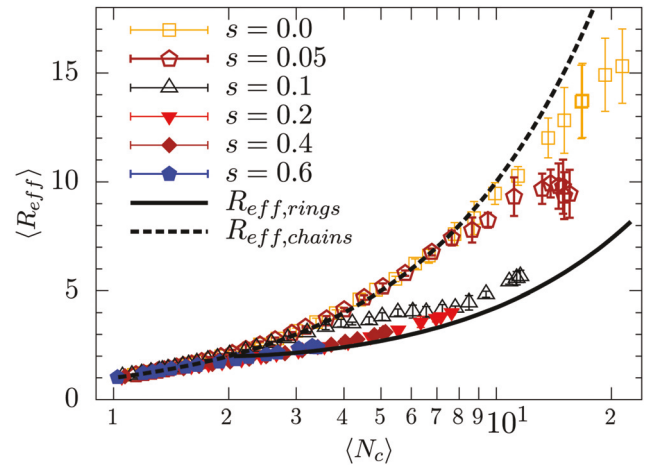


Fig. 6 Effective radius of clusters as a function of cluster size throughout the aggregation process. Also graphed as a solid black line and a dashed black line are the effective radius for ideally circular rings and straight chains, respectively.

systems. The radius of gyration $\langle R_{\rm g} \rangle$ shows essentially the same behavior as $\langle R_{\rm eff} \rangle$ when it's plotted as a function of $\langle N_{\rm c} \rangle$ (see Fig. S3 in the ESI†).

3.4 Combined effect of λ and shift

Fig. 7 shows the weight averaged mean cluster size at long times as a function of shift for various λ , also presented are the results of Yener *et al.*²² for 3D systems of $\phi = 0.07$ and $\lambda = 6.67-53.33$. Again the data in Fig. 7 represents the average of the last 20% of the simulations. Systems which are time-dependent are graphed

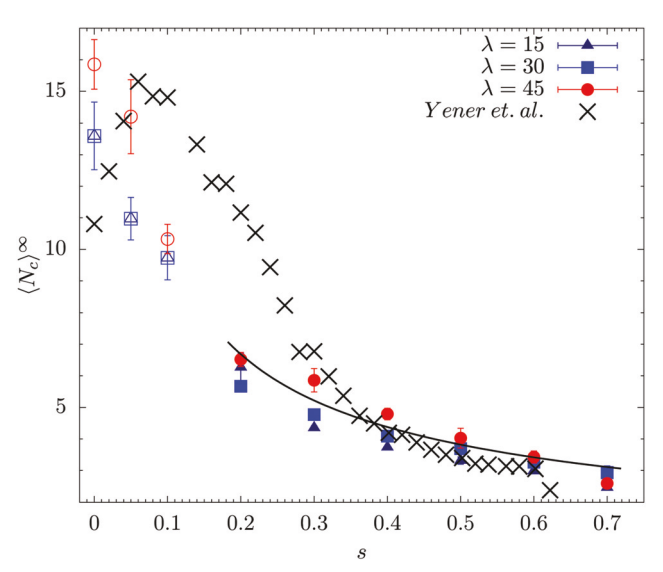


Fig. 7 Long time weight averaged mean cluster sizes, $\langle N_c \rangle^{\infty}$, as a function of dipolar shift for several magnetic coupling constant, λ . Filled symbols correspond to cases where the mean cluster size is time-independent, while open symbols correspond to cases where we observe time-dependency. A continuous line representing the power-law behavior of mean cluster size with respect to shift is shown for the time independent region. The results of Yener *et al.*²² for 3D systems of ϕ = 0.07 and λ = 6.67–53.33 are also graphed for comparison.

with open symbols since the values would differ depending on the final time simulated. For the region of systems that are timeindependent the average cluster size follows an inverse power law behavior with respect to the dipolar shift ($N_c \sim s^{-0.6\pm0.1}$). Since λ mainly serves to increase the rate of aggregation, its effect is more pronounced in the time-dependent systems as clusters will continue to grow until all particles form one cluster, while time-independent systems reach an equilibrium average cluster size where growth ceases. Comparison with the Yener results shows some deviation for low shift values as the average cluster size for these systems depends greatly on interaction strength, particle density and simulation time; all of which differ for our simulations, particularly the density (0.01 vs. 0.07) and simulation time (3000 vs. 7500). The 3D nature of the Yener's system allows for the formation of staggered loops in systems of shift 0.1-0.2, which contain a larger amount of average particles than the loops present in our simulations. The results are in agreement for shifts of 0.3 and higher where systems reach a given equilibrium size regardless of particle density or simulation time.

4 Conclusions

We studied the dynamics of magnetic Janus particles with differing combinations of dipolar shifts and magnetic interaction potentials. An inverse relationship was found between the lateral shift of the dipole and the average cluster size; as the dipole shift increases, the average cluster size decreases. Three basic cluster types were identified based on the dipolar shift: chains or loops, rings, and triplets or doublets; clusters characteristic of the low, medium and high shift regimes, respectively. Systems with shifts very close to 0 are time dependent because they favor chainlike aggregation, which allows for low-potential barriers to cluster growth, giving them a DLA nature that allows for continuous cluster growth. As the dipolar shift reaches 0.2 and beyond, the favorable orientation between dipoles of bonded particles leads clusters to contract, increasing the potential barrier for cluster growth such that the average cluster size reaches an equilibrium determined by the balance between attractive and repulsive forces. Our study of the effective radius as a function of cluster size shows that systems of shift higher than 0.2 exhibit clusters with great circularity, and there exists a transition point for systems of lower shift where they go from favoring linear structures to circular ones when clusters are large enough.

The main effect of λ increasing is a shorter aggregation time, though at high λ of over 75 cluster–cluster aggregation starts to happen for all systems, meaning that all systems become size dependent. Although our study did not consider the effects of hydrodynamic forces, it has been shown that even for systems of much higher particle concentration accounting for hydrodynamic forces does not change the qualitative nature of the system's aggregation. Understanding the factors that influence self-assembly can help characterize materials based on the geometry of their aggregation, or design them for specific uses

such as droplet manipulation or microfluidic mixing.^{35,36} The design process of new materials can also benefit from the fact that one can control the structures by tuning the parameters that affect self-assembly. Future work will include higher quantities and concentrations of particles, and three-dimensional simulations.

Conflicts of interest

There are no conflicts to declare.

Acknowledgements

This project was supported by the National Science Foundation under CAREER Award NSF-CBET 1055284 and 1705656, and the National Institute of Health under award T34GM008419.

References

- 1 O. A. Aktsipetrov, Colloids Surf., A, 2002, 202, 165-173.
- 2 A. Boymelgreen, G. Yossifon and T. Miloh, *Langmuir*, 2016, 32, 9540–9547.
- 3 L. Baraban, D. Makarov, O. G. Schmidt, G. Cuniberti, P. Leiderer and A. Erbe, *Nanoscale*, 2013, 5, 1332–1336.
- 4 B. Dai, J. Wang, Z. Xiong, X. Zhan, W. Dai, C.-C. Li, S.-P. Feng and J. Tang, *Nat. Nano*, 2016, **11**, 1087–1092.
- 5 C. Chen, F. Mou, L. Xu, S. Wang, J. Guan, Z. Feng, Q. Wang, L. Kong, W. Li, J. Wang and Q. Zhang, *Adv. Mater.*, 2017, 29, 1603374.
- 6 A. S. Lübbe, C. Alexiou and C. Bergemann, *J. Surg. Res.*, 2001, **95**, 200–206.
- 7 S. Singamaneni, V. N. Bliznyuk, C. Binek and E. Y. Tsymbal, J. Mater. Chem., 2011, 21, 16819.
- 8 J. J. Weis and D. Levesque, Phys. Rev. Lett., 1993, 71, 2729-2732.
- 9 P. J. Camp, J. C. Shelley and G. N. Patey, *Phys. Rev. Lett.*, 2000, **84**, 115–118.
- 10 L. Rovigatti, J. Russo and F. Sciortino, *Phys. Rev. Lett.*, 2011, 107, 237801.
- 11 L. Rovigatti, J. Russo and F. Sciortino, *Soft Matter*, 2012, **8**, 6310–6319.
- 12 W. L. Miller and A. Cacciuto, *Phys. Rev. E: Stat., Nonlinear, Soft Matter Phys.*, 2009, **80**, 021404.
- 13 J. H. Byeon and J. H. Park, Sci. Rep., 2016, 6, 35104.

- 14 P. Tierno, Phys. Chem. Chem. Phys., 2014, 16, 23515-23528.
- 15 B. Ren, A. Ruditskiy, J. H. Song and I. Kretzschmar, *Langmuir*, 2012, 28, 1149–1156.
- 16 A. Ruditskiy, B. Ren and I. Kretzschmar, *Soft Matter*, 2013, 9, 9174–9181.
- 17 J. J. Weis and D. Levesque, *Phys. Rev. Lett.*, 1993, 71, 2729–2732.
- 18 Z. Wang and C. Holm, Phys. Rev. E: Stat., Nonlinear, Soft Matter Phys., 2003, 68, 41401.
- 19 S. Kantorovich, R. Weeber, J. J. Cerda and C. Holm, *Soft Matter*, 2011, 7, 5217.
- 20 M. Klinkigt, R. Weeber, S. Kantorovich and C. Holm, *Soft Matter*, 2013, **9**, 3535–3546.
- 21 S. Kantorovich, E. Pyanzina and F. Sciortino, *Soft Matter*, 2013, 9, 6594–6603.
- 22 A. B. Yener and S. H. L. Klapp, *Soft Matter*, 2015, **12**, 2066–2075.
- 23 J. Dobnikar, A. Snezhko and A. Yethiraj, Soft Matter, 2013, 9, 3693.
- 24 A. Snezhko and I. S. Aranson, Nat. Mater., 2011, 10, 698-703.
- 25 F. Ginot, I. Theurkauff, F. Detcheverry, C. Ybert and C. Cottin-Bizonne, *Nat. Commun.*, 2018, 9, 696.
- 26 E. V. Novak, E. S. Pyanzina and S. S. Kantorovich, J. Phys.: Condens. Matter, 2015, 27, 234102.
- 27 N. M. Kovalchuk and V. M. Starov, Adv. Colloid Interface Sci., 2012, 179–182, 99–106.
- 28 A. Tomilov, A. Videcoq, M. Cerbelaud, M. A. Piechowiak, T. Chartier, T. Ala-Nissila, D. Bochicchio and R. Ferrando, J. Phys. Chem. B, 2013, 117, 14509–14517.
- 29 J. D. Weeks, D. Chandler and H. C. Andersen, *J. Chem. Phys.*, 1971, **54**, 5237–5247.
- 30 D. J. Evans, Mol. Phys., 1977, 34, 317-325.
- 31 D. J. Evans and S. Murad, Mol. Phys., 1977, 34, 327-331.
- 32 T. Edvinsson, P. J. RÅsmark and C. Elvingson, *Mol. Simul.*, 1999, 23, 169–190.
- 33 F. G. Pierce, Aggregation in colloids and aerosols, PhD thesis, Kansas State University, 2007.
- 34 M. Y. Lin, H. M. Lindsay, D. A. Weitz, R. C. Ball, R. Klein and P. Meakin, *Phys. Rev. A: At., Mol., Opt. Phys.*, 1990, 41, 2005–2020.
- 35 G. Huang, M. Li, Q. Yang, Y. Li, H. Liu, H. Yang and F. Xu, *ACS Appl. Mater. Interfaces*, 2017, **9**, 1155–1166.
- 36 M. Ballard, D. Owen, Z. G. Mills, P. J. Hesketh and A. Alexeev, *Microfluid. Nanofluid.*, 2016, **20**, 1–13.